VIP Nanoparticles Very Important Paper

International Edition: DOI: 10.1002/anie.201601016
German Edition: DOI: 10.1002/ange.201601016

Modulating fcc and hcp Ruthenium on the Surface of Palladium–Copper Alloy through Tunable Lattice Mismatch

Yancai Yao[+], Dong Sheng He[+], Yue Lin, Xiaoqian Feng, Xin Wang, Peiqun Yin, Xun Hong, Gang Zhou, Yuen Wu, and Yadong Li**

Abstract: *Herein, we report an epitaxial-growth-mediated method to grow face-centered cubic (fcc) Ru, which is thermodynamically unfavorable in the bulk form, on the surface of Pd–Cu alloy. Induced by the galvanic replacement between Ru and Pd–Cu alloy, a shape transformation from a Pd–Cu@Ru core–shell to a yolk–shell structure was observed during the epitaxial growth. The successful coating of the unconventional crystallographic structure is critically dependent on the moderate lattice mismatch between the fcc Ru overlayer and $PdCu_3$ alloy substrate. Further, both fcc and hexagonal close packed (hcp) Ru can be selectively grown through varying the lattice spacing of the Pd–Cu substrate. The presented findings provide a new synthetic pathway to control the crystallographic structure of metal nanomaterials.*

Metal nanoparticles (NPs) are emerging as a central nanomaterial for catalysis,[1] plasmonics,[2] sensing,[3] and so on. Many of them, such as Fe,[4] Ni,[5,6] Ag,[7] Au,[8,9] and Ru[10] NPs can exhibit multiple crystallographic structures (e.g. face-centered cubic (fcc), hexagonal close packed (hcp), and body-centered cubic (bcc)) under different conditions. In addition to the well-studied features, such as size, composition, and shape, the crystallographic structure of metal NPs can also critically influence their functionalities.[11–13] Achieving the crystallographic structure control of metal NPs which will enable us to better explore their properties is highly desired for synthetic methodology studies. Traditionally in the bulk form, the structural control of a metal usually relies on altering the temperature and pressure.[8] Such rigid and expensive tuning methods are not suitable for practical applications. At the nanoscale, however, the surface compression or tensile stress may play a critical role in directing the crystallographic structure.[14,15] For instance, driven by the minimization process of surface energy, solvent exchange will lead to the transformation from icosahedral Au_{13} clusters protected by dodecanethiol and triphenylphosphine to cuboctahedral structure protected by triphenylphosphine via structural rearrangement.[15] Though much effort has been made,[7,8] it still remains a great challenge to modulate the crystallographic structure of metal NPs through mild chemical methods.

Epitaxial growth is a versatile and facile approach to construct core–shell, yolk–shell, or hybrid structures by depositing a crystalline overlayer on a crystalline substrate.[16–19] Taking the substrate as a seed, the crystallographic structure of the overlayer usually preserves the same epitaxy with respect to the substrate in the case of moderate lattice mismatches between two materials. Otherwise, the overlayer is either differently orientated with respect to the substrate or randomly located on the surface of the substrate.[20] Under given temperature and pressure, the lattice mismatch between two materials is usually unchangeable. As such, modulating the epitaxial or non-epitaxial mode that the overlayer adopts to grow on the substrate cannot be implemented. An alloy is an exception, whereas its lattice parameter is tunable at some level by varying the composition ratio of two metals. This unique feature may impart flexibility to designing the lattice mismatch between the substrate and the overlayer and offer the ability to manipulate the growth mode of the overlayer.

Ruthenium is one of the most promising metal materials because of its importance in catalyzing a wide range of reactions, such as synthesis of ammonia,[21] Fischer–Tropsch synthesis,[21] and CO oxidation[22]/methanation.[23] Most recently, Joo and Kusada have discovered the existence of the nanoscale fcc Ru, which is not conventional and is not favored at ambient conditions, and reported its relative different catalytic performance with respect to the hcp Ru.[10,22] To date, the synthetic methodology of controlling the crystallographic structure of Ru or its heterostructures is still scarce.[24] Herein, we demonstrate the epitaxial growth can be utilized to induce the fcc Ru overlayer on the Pd–Cu alloy surface by carefully tuning the composition of bimetallic alloy substrate. In addition, when the composition ratio of Pd and Cu was varied, the enlarged lattice mismatch could not be compensated and the epitaxial growth was broken. Thus, the hcp Ru, which is the conventionally stable structure,[25] dominated at the overlayer. This is the first report that shows the modulating of the crystallographic structure of an

[*] Y. Yao,[+] D. S. He,[+] X. Feng, X. Wang, P. Yin, X. Hong, Y. Wu, Y. Li
Center of Advanced Nanocatalysis
University of Science and Technology of China (CAN-USTC)
Hefei, Anhui 230026 (P.R. China)
E-mail: yuenwu@ustc.edu.cn
ydli@mail.tsinghua.edu.cn

Y. Lin
Hefei National Laboratory for Physical Sciences at the Microscale, University of Science and Technology of China
Hefei, Anhui Province 230026 (P.R. China)

Y. Li
Department of Chemistry, Tsinghua University
Beijing 100084 (P.R. China)

G. Zhou
State Key Laboratory of Chemical Resource Engineering, Beijing University of Chemical Technology
Beijing 100029 (P.R. China)

[+] These authors contributed equally to this work.

Supporting information for this article can be found under: http://dx.doi.org/10.1002/anie.201601016.

 © 2016 Wiley-VCH Verlag GmbH & Co. KGaA, Weinheim

overlayer on the same type of substrate through tunable lattice mismatch.

Figure 1 illustrates the epitaxial growth of the fcc Ru shell on a Pd–Cu alloy seed and the shape transformation from Pd–Cu@Ru core–shell to yolk–shell architectures. The processes were traced by transmission electron microscopy (TEM) at three representative stages (0, 6, 12 hours). We first adopted a solvothermal method to synthesize $PdCu_3$ alloy seeds with

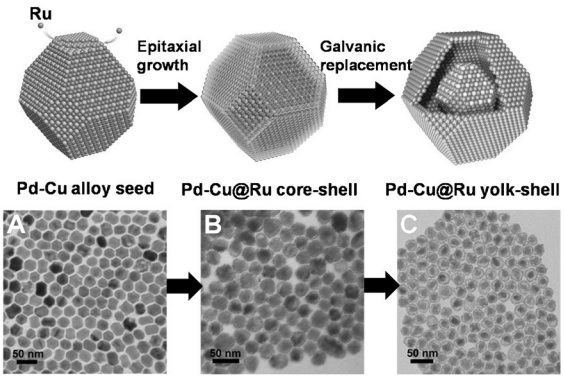

Figure 1. Schematic illustrations and corresponding TEM images of the samples obtained at three representative stages during the structure evolution process. A) $PdCu_3$ seed B) Pd–Cu@Ru core–shell NPs, and C) Pd–Cu@Ru yolk–shell NPs.

a homogeneous truncated octahedral shape and uniform size (19.6 ± 0.8 nm), as shown in Figure 1 A (the composition ratio was measured by inductively coupled plasma mass spectrometry (ICP-MS)). The epitaxial growth was initially induced by the galvanic replacement between Ru and $PdCu_3$ seeds, during which the Pd–Cu seeds gradually adopted a Pd–Cu@Ru core–shell structure (Figure 1 B). Evidenced by X-ray diffraction (XRD) spectra, no peak appears that can be assigned to hcp Ru and the peaks belonging to fcc $PdCu_3$ remained roughly unshifted throughout the entire process (Figure S1 in the Supporting Information). ICP-MS measurement showed that the Pd/Cu ratio was retained at nearly 1:3. Therefore, it was concluded that the Ru^{III} would gradually replace both the Pd^0 and Cu^0 during the evolution process (EDS results are shown in Figure S2 and S3). As shown in Figure 1 C, the galvanic replacement finally resulted in a well-defined Pd–Cu@Ru yolk–shell structure. The detailed one-to-one correspondence between the TEM images at the three reaction stages and the projections of the 3D models are depicted in Figure 1 according to our experimental results and hypotheses.

The aberration-corrected high-angle annular dark-field scanning transmission electron microscopy (HAADF-STEM) images showed that all of the initial $PdCu_3$ seeds were fcc (Figure S4). The corresponding elemental mappings revealed both Pd and Cu were uniformly distributed across the whole particle, in accordance with the nature of bimetallic alloy. The fast Fourier transforms (FFTs) ascribed to the atomic image of an individual $PdCu_3$ NP confirmed the standard fcc arrangement orientated along the [011] direction. According to the lattice spacing measurements in Figure S4-b, the average crystal constant of $PdCu_3$ (3.75 Å) was between that of Pd and Cu, which was consistent with the XRD measurement in Figure S1.

The detailed electron micrograph of Pd–Cu@Ru core–shell structure after adding $RuCl_3$ solution is shown in Figure 2 A,B. Indeed, the galvanic replacement between Ru and Pd was a slow process, which could be attributed to their roughly equivalent redox potentials. Alloying Pd with Cu would reduce its redox potential (Figure S5), which was beneficial for the galvanic replacement between the $PdCu_3$

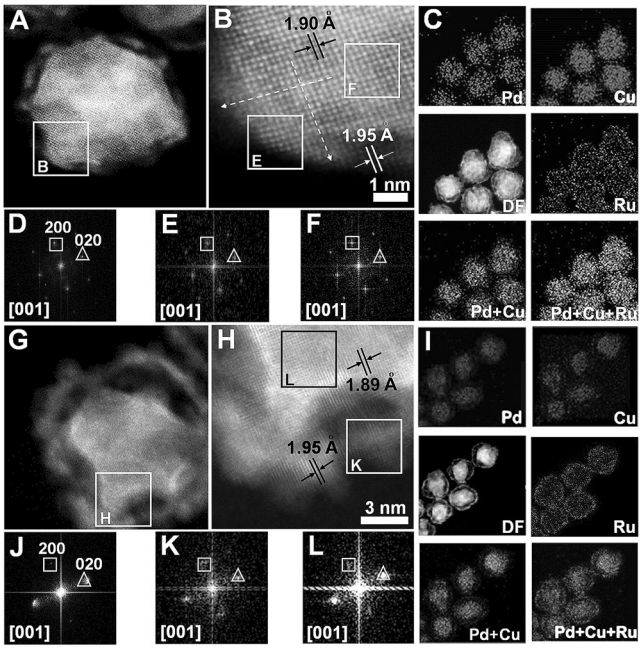

Figure 2. A,B) HAADF-STEM images, C) EDS mappings, and D,E,F) FFT patterns of Pd–Cu@Ru core–shell nanoparticles. G,H) HAADF-STEM images, I) EDS mappings, and J,K,L) FFT patterns of Pd–Cu@Ru yolk–shell nanoparticles. See text for details. DF = dark field.

seed and Ru.[26] Surprisingly, the crystallographic structure of the Ru overlayer grown on the $PdCu_3$ surface was fcc phase as verified by the atomic HAADF-STEM images (Figure 2 A,B). Indicated by the white dashed line in Figure 2 B, it was very clear that the lattice of overgrown layers followed that of the core, showing the overgrowth of Ru was in a cube-on-cube epitaxial fashion. The FFT of an individual particle revealed the pattern (Figure 2 D) was a standard fcc pattern along with the [001] zone axis. The FFT patterns taken from the regions of core (Figure 2 F) and shell (Figure 2 E), respectively, further confirmed the atoms in these two areas adopt the same stacking mode. It was worth pointing out that the lattice spacing of core (1.90 Å) was close to that of shell (1.95 Å), allowing the epitaxial growth of Ru on the $PdCu_3$ surface. The corresponding elemental mappings clearly illustrated the core–shell structure, in which Pd and Cu concentrate at the center and Ru atoms located at the shell.

When extending the reaction to 12 h, most NPs evolved into the unique yolk–shell shape, with an average core size of 14.9 ± 1.4 nm and shell thickness of 2.9 ± 0.5 nm (Figure 2 G). The key in the formation of yolk–shell structure was the

 © 2016 Wiley-VCH Verlag GmbH & Co. KGaA, Weinheim

difference of the diffusion rate, which could be referred as Kirkendall effect.[27] Pd and Cu atoms diffused outwards faster than the inward diffusion of Ru atoms. This difference generates a net flux of vacancies from the surface to the center. The vacancies then coalesce into voids and develop preferably at the interface of the shell and core, which enables the formation of yolk–shell structure. Once the Ru atoms started to grow on the surface of $PdCu_3$, the newly deposited surface Ru atoms would serve as more tendentious deposition sites relative to $PdCu_3$ for further nucleation of Ru atoms. The HAADF-STEM image (Figure 2H) of an individual NP suggested that Ru overlayer maintained the fcc atom packing throughout the structural evolution process, which is also supported by a sole set of diffraction patterns in the corresponding FFT pattern (Figure 2J). To better strengthen this conclusion, we further compared two one-to-one FFTs of selected core and shell regions separately, thus reconfirming that the fcc overlayer can be induced by epitaxial growth on an fcc substrate (Figure 2K,L). Carefully examinations at different areas confirmed the thickness of the Ru shells was mostly below 3 nm and the crystal phase adopts the fcc structure (Figure S6). The corresponding elemental mappings were measured to clarify the spatial distribution of this trimetallic structure. Clearly shown in Figure 2I, that the Pd–Cu alloy core is at the center of the hollow Ru shell with a clear gap between core and shell.

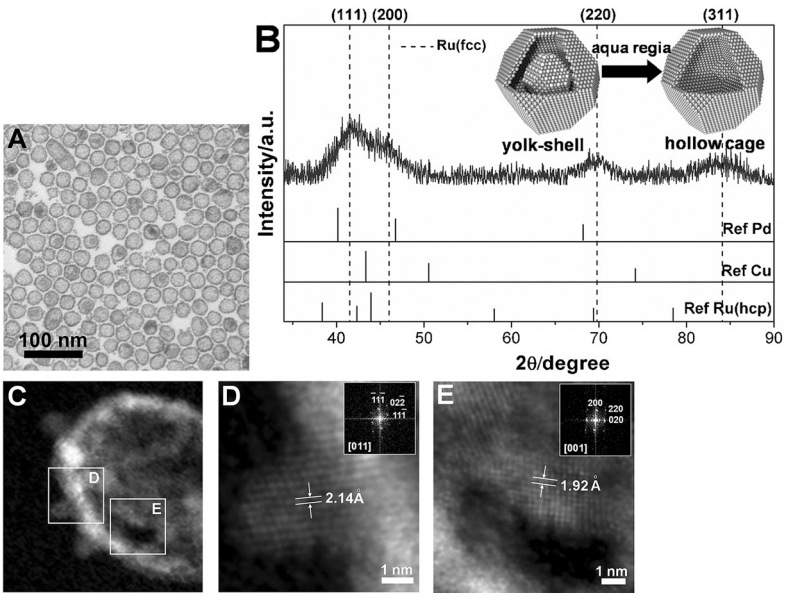

Figure 3. A) TEM image, B) XRD pattern, and C,D,E) HAADF-STEM images (insets are corresponding FFT patterns) of Ru hollow cage

To reinforce that the fcc Pd–Cu alloy was encapsulated by the fcc Ru shell, we conducted an element-selective etching process to elucidate the real shape and crystallographic structure. In detail, the Ru was separated from the Pd and Cu through to its insolubility in aqua regia (HNO_3/HCl), leaving a residual hollow Ru cage (Figure 3A). This process could be accurately traced by the line-scan profile in Figure S7 and EDS spectra in Figure S8, indicating the dissolution of the Pd–Cu core. The crystallographic structure of the hollow cage was identified by XRD (Figure 3B) and high resolution HAADF-STEM images (Figure 3C,D,E). The low-index XRD peaks revealed that the crystallographic structure of Ru hollow cage was fcc phase, which was in line with the previously discussion. The broadness of the peaks matched the HAADF-STEM observation of the hollow Ru NP in Figure 3C very well, which shows that the Ru shell was as thin as 2–4 nm. The high resolution HAADF-STEM images (Figure 3D,E) together with their FFTs from two selected areas also evidenced the characteristic fcc orientation along the [011] and [001] directions, respectively.

We further explored the crystallographic structure of grown Ru overlayer on a variety of comparable Pd–Cu alloy surface. They were synthesized using the same method with different ratios of Pd and Cu precursors. According to the Vegard's law,[28] the lattice parameter of the Pd–Cu alloy would change correspondingly by varying the composition ratio of Pd and Cu, which gave the ability to tune the lattice spacing ranging from that of Pd to that of Cu. Figure S9 shows the TEM images of composition-dependent Pd–Cu alloy seeds with comparable morphology and size. The XRD patterns, as shown in Figure S10, evidenced that the peaks indexed to {111}, {200}, and {220} diffractions of fcc structure situated between the standard fcc Pd and Cu and gradually left-shifted with the increasing Pd concentration. When Ru was deposited on those seeds, a different crystallographic structure of the Ru shell could be selectively obtained, whose XRD spectra (after treatment with aqua regia) are shown in Figure 4A. Lattice mismatch is defined as the atomic distance ratio of Ru to Pd–Cu alloy. By building modes, the estimated lattice mismatch between (hcp and fcc) an Ru layer and Pd–Cu alloys is shown in Figure 4B. In addition, we try to confirm the role of lattice mismatch on the structural preference of different ratio of Pd–Cu alloy. Pd–Cu seeds with a minor lattice mismatch with respect to fcc Ru, such as $PdCu_3$ and $PdCu_{2.5}$ were beneficial for the growth of a fcc Ru shell, in agreement with the HRTEM observations (Figure S11). The deviation from the fcc Ru, no matter whether in higher or smaller concentration, such as Pd (Figure S12, S13), $PdCu_2$ (Figure S14), or Cu (Figure S15–S17), would drive the generation of the dominant hcp Ru. That is, once the lattice mismatch was increased to demolish the epitaxial growth, the Ru overlayer would transform to its conventional hcp structure.

From the viewpoint of energetics, the stability of the epitaxial film or the determination of growth modes could be evaluated by the binding energy of two parts, that is, the competition between chemical bonding energy, contributed by new bonds across the interface, and the elastic energy, caused by lattice mismatch.[29,30] Density functional theory (DFT) calculations in the slab periodic model showed that the lattice constant of fcc Ru layers was 3.75 Å, very close to the experimental value (3.80 Å). The calculated binding energy of fcc Ru on the $PdCu_3$(001) surface (−6.85 eV/Ru atom) is far stronger than those of fcc Ru and hcp Ru on $PdCu_3$(111)

 © 2016 Wiley-VCH Verlag GmbH & Co. KGaA, Weinheim

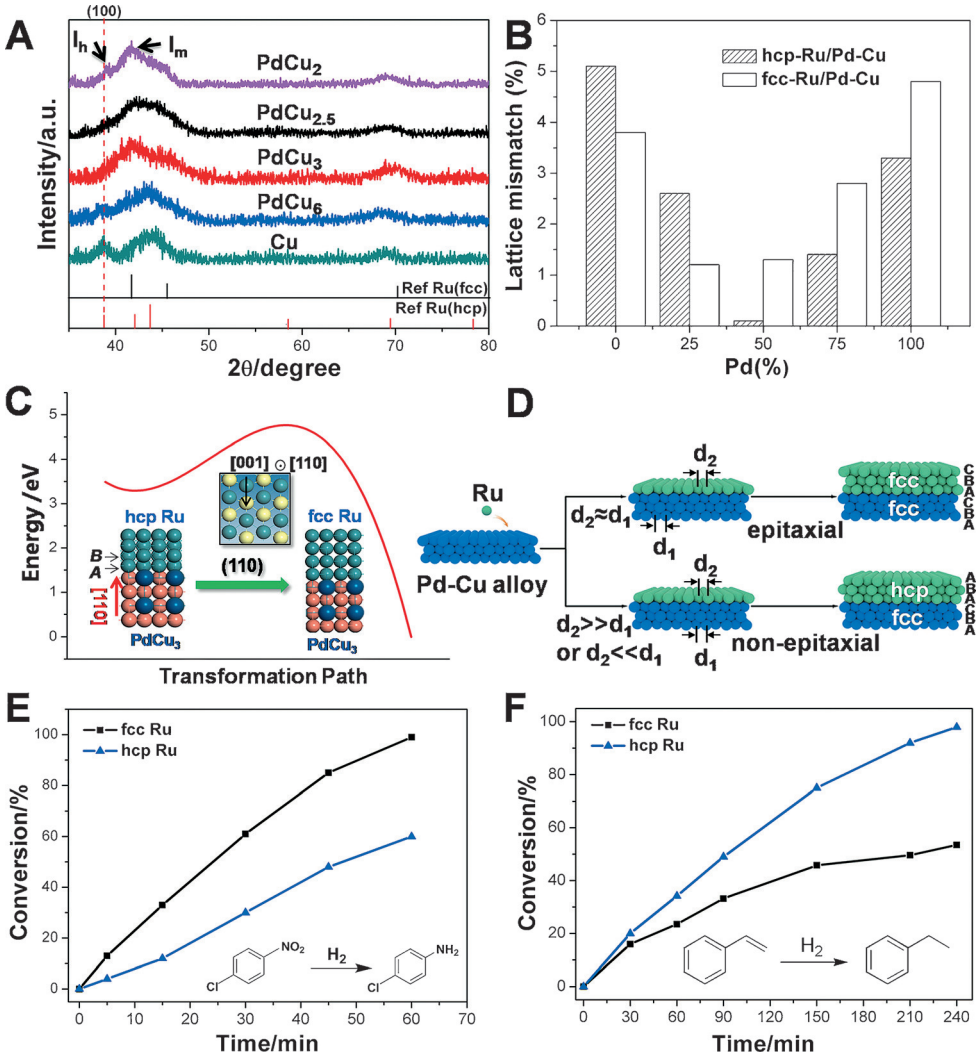

Figure 4. A) XRD spectra of Pd–Cu@Ru nanoparticles after treatment with aqua regia. The Pd/Cu ratios within the initial seed are 1/2, 1/2.5, 1/3, 1/6, and 0/1, respectively (From top to bottom). B) Lattice mismatch between (hcp and fcc) Ru and Pd–Cu alloys with the content of Pd. C) Structural transformation of hcp Ru to fcc Ru on the $PdCu_3$ substrate driven by the elastic energy, caused by lattice mismatch. Green, blue and red balls correspond to Ru, Pd, and Cu atoms, respectively. D) Schematic illustrations of the epitaxial and non-epitaxial growth of Ru on a Pd–Cu surface. E) Hydrogenation of 4-nitrochlorobenzene and F) hydrogenation of styrene catalyzed by hcp Ru and fcc Ru.

ones (−4.34 and −4.66 eV/Ru atom; Figure S19). So in what follows, we focus on the situation of Ru on the exposed (001) facet of truncated octahedral $PdCu_3$, as verified by TEM (see Figure 1).

The lattice mismatch between fcc Ru(001) and $PdCu_3$(001) was 0.54%, only producing an elastic energy of 0.11 eV. In contrast, the binding energy of fcc Ru(001) to $PdCu_3$(001) surfaces was estimated to be up to −13.04 eV. In this manner, the contribution from the lattice mismatch was less important, and consequently, the chemical bonding energy dominated the nucleation behavior of Ru on the $PdCu_3$ substrate with epitaxial growth of Ru with the same structure as the $PdCu_3$ substrate. So the growth proceeded in a layer-by-layer fashion, just as in our experimental observations.

By comparison, the nucleation behavior of hcp Ru on a $PdCu_3$(001) substrate was more complicated because an ideal coherent interface was extremely difficult to achieve. To minimize the surface energy of the substrate, the nucleation in general required the reduced Ru atoms to bind to the surface atoms as much as possible, showing an ideal coherent interface.[31] This allows, to the greatest extent possible, the contacting hcp Ru to have the same number of and similar arrangement of atoms as the $PdCu_3$(001) surface, typically the (110) surface. The calculated surface lattice constants of hcp Ru(110) were 4.28 Å and 4.64 Å, much larger than that of $PdCu_3$-(001). More precisely, the lattice mismatches along the [100] and [010] directions of the $PdCu_3$(001) substrate were up to 14.6% and 24.4%, respectively. Our further dynamics simulations illustrated that upon the nucleation assumed in epitaxial growth, the induced elastic energy was estimated to reach 6.39 eV, and completely counteract the stacking energy difference of −1.66 eV between the hcp Ru and fcc Ru structures. As a consequence, under induced stress conditions, the Ru atoms at the interface (A layer; green in top inset of Figure 4C) moved along the [001] direction, and subsurface Ru atom (B layer, yellow in top inset of Figure 4C) upshifted along the [110] direction. Finally, the hcp to fcc structure transformation was induced (Figure 4C). Even so, the structural transformation, driven by thermodynamics as there was a rather large contribution of the lattice mismatch energy to the Gibbs free energy, was not spontaneous, and needed to overcome a barrier of at least 1.15 eV (the red curve in Figure 4C). All of these evidence showed that too large a lattice mismatch would effectively hinder the nucleation of hcp Ru on the $PdCu_3$(001) substrate, causing a polycrystal Ru overlayer (Figure 4D). In principle, the mechanism for the instability of an interface induced by the tensile surface-stress was very similar to the Asaro–Tiller–Grinfeld (ATG) instability.[32,33]

In addition, the analysis based on DFT calculations also indicates that for other Pd–Cu alloys, the advantage of the (smaller) lattice mismatch (and/or stronger binding energy)

 © 2016 Wiley-VCH Verlag GmbH & Co. KGaA, Weinheim

allows the epitaxial growth of inherently stable hcp Ru overlayers rather than inherently unstable fcc Ru ones (Figure 4B, Figure S20). All of these features are consistent with the experimental observations.

To further explore the structure–activity relationship between catalytic behavior and crystallographic phase, hcp-dominated Ru catalysts prepared from Cu NPs (defined as hcp Ru) were compared with fcc-dominated Ru. We performed the hydrogenation of 4-nitrochlorobenzene and styrene as probe reactions to investigate these two samples. In the hydrogenation of 4-nitrochlorobenzene, the fcc Ru catalyst gave more activity with over 99% conversion of 4-nitrochlorobenzene in 60 min. In contrast, only 61% conversion was achieved by the hcp-dominated Ru (Figure 4E). However, the opposite trend, that hcp Ru exhibit higher activity than fcc Ru was observed in the hydrogenation of styrene (Figure 4F). The conversion of styrene was over 98% catalyzed by hcp Ru NPs compared with 53% conversion with fcc Ru NPs catalyst. This catalytic difference may be a result of the different adsorption behavior of the substrates on fcc and hcp Ru NPs. Importantly, in the semi-hydrogenation of diphenylacetylene the over-reduction product can be largely depressed by both the fcc and hcp Ru, which may result from poisoning effects by the generation of an Ru substrate complex on the surface. Moreover, the stereo selectivities of *cis*-stilbene can be maintained both by the hcp and fcc Ru catalysts (Figures S21,S22).

To conclude, it has been demonstrated that the lattice parameter plays a crucial role in controlling the crystallographic structure of Ru on the surface of Pd–Cu alloy. By optimizing the lattice parameter of the Pd–Cu alloy substrate, we are able to induce the unconventional fcc Ru overlayer by epitaxial growth, accompanied by a transformation from a trimetallic core–shell to yolk–shell structure. The trigger of epitaxial growth can be modulated by tuning the lattice mismatch between the alloy substrate and the overlayer, which enables the selective preparation of fcc or hcp Ru phases. Our findings provide a novel strategy to design multifunctional nanomaterials, simultaneously realizing composition, shape, and crystallographic structure control.

Acknowledgements

This work was supported by the Fundamental Research Funds for the Central Universities (WK2060190043), National Natural Science Foundation of China (U1463202, 21541004, and 21431003), State Key Project of Fundamental Research for Nanoscience and Nanotechnology (2011CB932401 and 2011CBA00500), National key Basic Research Program of China (2012CB224802). D.S.H. acknowledges the sponsorships of the Scientific Research Foundation for the Returned Overseas Scholars, Ministry of Education of China, and China Postdoctoral Science Foundation.

Keywords: crystallographic control · epitaxial growth · fcc ruthenium · lattice mismatch · nanoparticles

How to cite: *Angew. Chem. Int. Ed.* **2016**, *55*, 5501–5505
Angew. Chem. **2016**, *128*, 5591–5595

[1] J. K. Nørskov, T. Bligaard, B. Hvolbæk, F. Abild-Pedersen, I. Chorkendorff, C. H. Christensen, *Chem. Soc. Rev.* **2008**, *37*, 2163.
[2] M. Pelton, J. Aizpurua, G. Bryant, *Laser Photonics Rev.* **2008**, *2*, 136.
[3] G. Doria, J. Conde, B. Veigas, L. Giestas, C. Almeida, M. Assunção, J. Rosa, P. V. Baptista, *Sensors* **2012**, *12*, 1657.
[4] T. Ling, L. Xie, J. Zhu, H. Yu, H. Ye, R. Yu, Z. Cheng, L. Liu, L. Liu, G. Yang, *Nano Lett.* **2009**, *9*, 1572.
[5] C. Kim, C. Kim, K. Lee, H. Lee, *Chem. Commun.* **2014**, *50*, 6353.
[6] V. Tzitzios, G. Basina, M. Gjoka, V. Alexandrakis, V. Georgakilas, D. Niarchos, N. Boukos, D. Petridis, *Nanotechnology* **2006**, *17*, 3750.
[7] X. Liu, J. Luo, J. Zhu, *Nano Lett.* **2006**, *6*, 408.
[8] X. Huang, S. Li, Y. Huang, S. Wu, X. Zhou, S. Li, C. L. Gan, F. Boey, C. A. Mirkin, H. Zhang, *Nat. Commun.* **2011**, *2*, 292.
[9] J. Wu, W. X. Shi, S. Z. Li, C. L. Gan, H. Zhang, *Nat. Commun.* **2015**, *6*, 6571.
[10] K. Kusada, H. Kobayashi, T. Yamamoto, S. Matsumura, N. Sumi, K. Sato, K. Nagaoka, Y. Kubota, H. Kitagawa, *J. Am. Chem. Soc.* **2013**, *135*, 5493.
[11] L. Pust, L. E. Wenger, R. A. Lukaszew, Y. Sheng, D. Litvinov, Y. Wang, C. Uher, R. J. Clarke, *Appl. Phys.* **1999**, *85*, 5765.
[12] J. Kim, Y. Lee, S. Sun, *J. Am. Chem. Soc.* **2010**, *132*, 4996.
[13] J.-X. Liu, H.-Y. Su, D.-P. Sun, B.-Y. Zhang, W.-X. Li, *J. Am. Chem. Soc.* **2013**, *135*, 16284.
[14] J. Wu, P. Li, Y.-T. F. Pan, S. Warren, X. Yin, H. Yang, *Chem. Soc. Rev.* **2012**, *41*, 8066.
[15] Y. Li, H. Cheng, T. Yao, Z. Sun, W. Yan, Y. Jiang, Y. Xie, Y. Sun, Y. Huang, S. Liu, *J. Am. Chem. Soc.* **2012**, *134*, 17997.
[16] L. Manna, E. C. Scher, L.-S. Li, A. P. Alivisatos, *J. Am. Chem. Soc.* **2002**, *124*, 7136.
[17] J. Liu, S. Z. Qiao, J. S. Chen, X. W. D. Lou, X. Xing, G. Q. M. Lu, *Chem. Commun.* **2011**, *47*, 12578.
[18] D. He, Y. Han, J. Fennell, S. Horswell, Z. Li, *Appl. Phys. Lett.* **2012**, *101*, 113102.
[19] J. Gu, Y. Guo, Y.-Y. Jiang, W. Zhu, Y.-S. Xu, Z.-Q. Zhao, J.-X. Liu, W.-X. Li, C.-H. Jin, C.-H. Yan, *J. Phys. C* **2015**, *119*, 17697.
[20] J. Zhang, Y. Tang, K. Lee, M. Ouyang, *Science* **2010**, *327*, 1634.
[21] G. A. Somorjai, Y. Li, *Introduction to surface chemistry and catalysis*, Wiley, Hoboken, **2010**.
[22] S. H. Joo, J. Y. Park, J. R. Renzas, D. R. Butcher, W. Huang, G. A. Somorjai, *Nano Lett.* **2010**, *10*, 2709.
[23] R. A. Dagle, Y. Wang, G.-G. Xia, J. J. Strohm, J. Holladay, D. R. Palo, *Appl. Catal. A* **2007**, *326*, 213.
[24] J. E. Macdonald, M. B. Sadan, L. Houben, I. Popov, U. Banin, *Nat. Mater.* **2010**, *9*, 810.
[25] G. Rakhtsaum, *Platinum Met. Rev.* **2013**, *57*, 202.
[26] Y. Wu, D. Wang, Z. Niu, P. Chen, G. Zhou, Y. Li, *Angew. Chem. Int. Ed.* **2012**, *51*, 12524; *Angew. Chem.* **2012**, *124*, 12692.
[27] Y. Yin, R. M. Rioux, C. K. Erdonmez, S. Hughes, G. A. Somorjai, A. P. Alivisatos, *Science* **2004**, *304*, 711.
[28] A. R. Denton, N. W. Ashcroft, *Phys. Rev. A* **1991**, *43*, 3161.
[29] A. Danescu, *Int. J. Solids Struct.* **2001**, *38*, 4671.
[30] J. Stangl, V. Holý, G. Bauer, *Rev. Mod. Phys.* **2004**, *76*, 725.
[31] A. Trampert, *Physica E* **2002**, *13*, 1119.
[32] D. Jesson, K. Chen, S. Pennycook, T. Thundat, R. Warmack, *Phys. Rev. Lett.* **1996**, *77*, 1330.
[33] M. Grinfeld, *Thermodynamic Methods in the Theory of Heterogeneous Systems*, Longman Scientific and Technical, **1991**.

Received: January 28, 2016
Published online: March 24, 2016

 © 2016 Wiley-VCH Verlag GmbH & Co. KGaA, Weinheim